Detecting remote synchronization from empirical data of brain networks

Dehua Chen,[1] Zhiyin Yang,[1] Zhaohua Lin,[2] Guoshen Liang,[1] Wenbin Mao,[1] and Zonghua Liu[1,*]
[1]*School of Physics, East China Normal University, Shanghai 200241, People's Republic of China*
[2]*School of Medical Imaging, Fujian Medical University, Fuzhou 350100, People's Republic of China*

(Received 24 May 2026; accepted 30 August 2026; published 14 September 2026)

The emergence of functional connectivity between distant brain regions that lack a direct structural link remains a long-standing question in neuroscience. Remote synchronization (RS) offers a promising framework for uncovering the underlying mechanisms. So far, RS has been well studied in artificial network topologies such as star or starlike graphs but little attention has been paid to realistic brain networks with complicated topologies, due to their completely different synchronization pathways. In this study, we address this gap by introducing an efficient method, termed *the noncompletely overlapping path algorithm*, to detect RS using empirical structural and functional brain network data. Under this approach, two nodes are considered to exhibit RS if they are functionally synchronized despite being structurally disconnected. That is, they share neither a direct structural link nor an indirect path composed of synchronized nodes. We demonstrate that the proportion of RS nodes in a brain network strongly depends on the thresholds used to define both structural and functional connectivity, with optimal threshold values existing for each. Furthermore, we show that the method can be generalized: It applies not only to empirical time series but also to oscillator-based network models, and it admits a theoretical interpretation. This indicates that the algorithm offers a general framework to detect RS in complex networks.

DOI: 10.1103/tmkq-33c4

I. INTRODUCTION

Brain networks are broadly categorized into two distinct types: structural networks and functional networks. Structural networks may differ from species and exhibit exponential, small-world, or scale-free traits, whereas functional networks follow an approximately scale-free distribution [1]. Notably, functional connections can emerge between distant brain regions that lack a direct structural link [2,3], in contrast to the cases of long-range functional coupling, mediated synchronization, or topological distance effects. Thus, this specific functional correlation is in fact a phenomenon of remote synchronization (RS), where the correlation between two distant nodes arises from neither a direct structural connection nor any synchronized chains between them [4]. This raises a fundamental question: How do such functional connections or RS arise from the underlying structural architecture? Although this problem has recently attracted considerable interest [5–10], a complete understanding remains elusive.

At the microscopic level, the structural network of the brain comprises approximately 860 billion neurons, along with their axons and dendrites. Here, neurons function as network nodes, while axons and dendrites form the connections. Due to the enormous number of neurons, it is impractical to study them comprehensively through either experimental methods or numerical simulations. A feasible alternative is to shift to a mesoscopic scale, where each region of interest (ROI) is treated as a single node. This reduces the number of network nodes, N, to the order of hundreds or thousands. At this scale, the weight of a connection between two ROIs in the structural brain network can be quantified by the number of neural fibers identified using tractography algorithms [11].

In contrast to brain structural networks, brain functional networks are defined by synchronization between nodes. Evidence from both electroencephalography and magnetoencephalography indicates that the synchronization of neural activity across distant brain regions is crucial for functional interaction, with neuronal coherence serving as a key underlying mechanism [12,13]. For instance, synchronous neural firing in the gamma frequency band has been linked to visual awareness [14], while the slow waves of sleep synchronize cortical regions with high precision and can recruit multiple subcortical targets [15]. Furthermore, long-range synchronization of oscillatory signals is thought to mediate interactions within large-scale cortical networks, indicating that oscillatory synchronization is fundamentally organized at this scale [16]. On the other hand, abnormal synchronization is closely associated with brain network dysfunction, such as the aberrant synchrony in epilepsy [17,18]. Specifically, this phenomenon can be leveraged for medical diagnosis, such as distinguishing between children with attention deficit hyperactivity disorder and healthy children [19,20].

Although these evidences come from diverse aspects of brain activity, they converge on a central principle: Specific brain functions are activated not by the entire brain, but by particular sets of neurons. These sets form rhythmically activated and inhibited cognitive networks dedicated to specific functions [21]. Broadly, the brain can be studied in two primary states: resting and task based. During the resting state,

*Contact author: zhliu@phy.ecnu.edu.cn

spontaneous brain fluctuations are not random but highly structured, forming spatial patterns of correlated activity across different regions known as resting-state networks (RSNs). These include the attention, frontoparietal, default-mode networks, etc. [22–25]. During task-based cognition, invasive recordings reveal task-specific synchronization between focal cortical sites [26].

In sum, the structural and functional networks of the human brain are fundamentally distinct. During adulthood, the structural network, composed of all 860 billion neurons, remains largely stable over years or even decades. In contrast, the functional network involves only a subset of neurons, is time dependent, and continuously shifts between different cognitive states [12,27]. To understand how functional networks emerge from the structural substrate, a promising framework is RS in star-graph networks, introduced by Bergner *et al.* in 2012 [4]. They demonstrated that indirectly connected leaf nodes can synchronize, whereas directly connected hub and leaf nodes do not, provided that the hub's natural frequency differs significantly from that of the leaves [9,10]. Subsequently, RS has been extensively studied in various starlike networks [28–34]. This concept was later extended to complex networks [35], in which nodes with high degrees are treated as hubs with high natural frequencies, and those with lower degrees as leaves with low natural frequencies—representing a bimodal frequency distribution.

However, the mechanism of RS derived from star-graph networks cannot be directly extended to brain networks, for two main reasons. First, in star graphs, RS occurs between local nodes via a central hub, whereas in brain networks, RS typically arises between distant nodes without the mediation of a hub. Second, the RS of star graph requires a marked difference between the natural frequencies of the hub and leaf nodes, allowing the hub to act as a relay. In contrast, brain networks are generally assumed to exhibit homogeneous nodal natural frequencies; currently, there is no evidence indicating substantial heterogeneity in the natural frequencies of neurons. Therefore, explaining the mechanism underlying RS in realistic brain systems remains an open question.

In this work, we address this problem by analyzing empirical data from both brain structural and functional networks. This data-driven approach allows us to circumvent the limitations of the star-graph model, i.e., the requirement of a hub-mediated topology and a significant frequency difference between hub and leaf nodes. We introduce an effective method for detecting RS directly from empirical structural and functional network data. Our analysis reveals that the fraction of nodes exhibiting RS depends critically on the threshold choices for both structural and functional connectivity, and that optimal thresholds exist for each network type. Furthermore, we demonstrate that this method can be extended to oscillator-based brain network models and is supported by theoretical reasoning, indicating its generality for detecting RS in complex networks.

II. AN EFFECTIVE APPROACH TO DETECT REMOTE SYNCHRONIZATION IN BRAIN NETWORKS

As discussed above, the functional network of brain arises from the underlying structural network, yet the precise mechanism of this emergence remains unclear. To address this, we examine the underlying dynamics at different scales. At the microscopic scale, the structural network consists of neurons as nodes, interconnected by axons and dendrites. Within such a network, the dynamics of each node are significantly influenced by all other nodes through network coupling. When the coupling strength is positive and moderately large, collective network behavior can emerge. As coupling increases further, various dynamic patterns may arise, corresponding to different cognitive networks. Excessively strong coupling, however, can induce abnormal synchronization, a state associated with epileptic seizures. Given the impossibility of recording the activity of all billions of individual neurons, we shift to the mesoscopic scale, where networks are defined by hundreds to thousands of ROIs. This scale remains computationally and experimentally tractable while preserving essential network dynamics.

In details, we first measure the time series $x(i,t)$ of each node (ROI), with $i = 1, 2, \ldots, N$ being the node index and N being the total number of nodes in the structural brain network. These nodes also serve as the nodes of the functional network. To obtain the links of functional network, we compute the Pearson correlation coefficients between the time series of any two nodes i and j by the following formula [1]:

$$F(i,j) = \frac{\langle (x(i,t) - \langle x(i,t)\rangle)(x(j,t) - \langle x(j,t)\rangle)\rangle}{\sigma(x(i))\sigma(x(j))}, \quad (1)$$

where $\langle x(i,t)\rangle$ denotes the temporal average of $x(i,t)$, $\sigma^2(x(i)) = \langle (x(i,t) - \langle x(i,t)\rangle)^2\rangle$, and $\langle\cdot\rangle$ represents temporal averaging. The coefficient $F(i,j)$ lies between -1 and 1, with $F(i,j) = 1, 0$, and -1 corresponding to perfect positive linear correlation, no linear correlation, and perfect negative linear correlation, respectively. Subsequently, a threshold F_c is introduced: A functional link between nodes i and j is considered present if their correlation $F(i,j)$ exceeds the threshold, regardless of whether a direct structural connection exists. Through this procedure, the resulting functional network depends on the choice of F_c and is fundamentally distinct from the underlying structural network [1]. For example, studies have reported that in the resting state, only about 30% of functional connectivity can be attributed to direct white-matter pathways, whereas the remaining 70% arises between regions without direct anatomical links [36].

Generally, the resulting brain functional network is time dependent and effectively represents a cognitive network. Here, we examine RS within such cognitive networks, which often comprise several communities, such as the attention, frontoparietal, and medial default-mode networks. In these networks, a functional link may or may not coincide with an underlying structural connection. We are particularly interested in functional connections that lack corresponding structural links. To determine whether a functional connection between two distant nodes constitutes RS, the following two conditions must be satisfied: (1) There must be no direct structural connection between the two nodes, regardless of their spatial proximity. Otherwise, the observed synchronization would be direct, not remote. (2) There should be no chain of synchronized nodes linking the two nodes; otherwise, synchronization could propagate stepwise along the chain, which

would not qualify as RS. In summary, a functional connection is classified as RS only when both of these criteria are met.

Based on this analysis, we now propose a general method to detect RS between any two nodes i and j. The central idea rests on the noncomplete overlap between structural and functional connections; we therefore term it the *noncomplete overlapping path algorithm* (NCOPA). The procedure is outlined below:

(1) Determine the threshold matrices of brain structural and functional networks by given thresholds. Given a weighted structural network $S = (S(i, j))$, we set a threshold S_c and define the corresponding binary structural matrix $\mathrm{SC} = (\mathrm{SC}(i, j))$ as follows: $\mathrm{SC}(i, j) = 1$ if $S(i, j) > S_c$ and $\mathrm{SC}(i, j) = 0$ otherwise for $i, j = 1, \ldots, N$. Thus, SC is the thresholded structural connectivity matrix. Similarly, for the measured functional network $F = (F(i, j))$ obtained from Eq. (1), we apply a threshold F_c and define the binary functional matrix $\mathrm{FC} = (\mathrm{FC}(i, j))$ as $\mathrm{FC}(i, j) = 1$ if $F(i, j) > F_c$ and $\mathrm{FC}(i, j) = 0$ otherwise for $i, j = 1, \ldots, N$. The resulting matrix FC represents the thresholded functional connectivity. Both binary matrices are of size $N \times N$, where N is the total number of nodes.

(2) Determine the optimal thresholds. We vary the thresholds S_c and F_c to generate a series of corresponding binary structural matrices SC and functional matrices FC. The thresholds are considered optimal, or within the optimal range, when the resulting matrices align with known empirical properties. For example, in Ref. [1], the optimal thresholds yield an approximate Gaussian distribution for structural connections and an approximate power-law distribution for functional connections. For other cases, however, the choice of SC and FC thresholds may need to be modified accordingly.

(3) Generate an overlapping matrix. Based on the obtained optimal threshold matrices SC and FC, we construct an overlap matrix $\mathrm{OC} = (\mathrm{OC}(i, j))$ to identify connections that are present in both networks. The elements of OC are defined for all $i, j = 1, \ldots, N$ as $\mathrm{OC}(i, j) = 1$ if both $\mathrm{SC}(i, j) = 1$ and $\mathrm{FC}(i, j) = 1$ and $\mathrm{OC}(i, j) = 0$ otherwise. Thus, $\mathrm{OC}(i, j) = 1$ indicates that a link between nodes i and j exists simultaneously in the binarized structural and functional networks, while $\mathrm{OC}(i, j) = 0$ denotes the absence of such an overlapping connection.

(4) Determine RS connection by two necessary conditions. Condition 1 (structural-functional mismatch): For the selected node pair (i, j), no direct structural link exists ($\mathrm{SC}(i, j) = 0$), but a functional link is present ($\mathrm{FC}(i, j) = 1$). Condition 2 (no overlapping path): There is no path between nodes i and j in the overlap matrix OC. A pair (i, j) is classified as exhibiting RS if and only if both conditions are satisfied.

Following these four steps, all instances of RS can be identified by exhaustively examining all node pairs in the structural and functional networks. A schematic illustration of the algorithm is presented in Fig. 1, where the top node i and bottom node j are the pair under evaluation, the intermediate nodes represent possible relay nodes, and black, blue, and red lines denote structural (SC), functional (FC), and overlapping (OC) connections, respectively. Specifically, Figs. 1(a)–1(c), respectively, show the networks corresponding to SC, FC, and OC, while Fig. 1(d) integrates all connections from the three panels. In Fig. 1(a), nodes i and j are connected via the structural network but not directly linked. Figure 1(b) indicates that i and j are functionally connected, while none of the intermediate nodes are functionally connected to both. Figure 1(c) confirms that there is no path between i and j in the overlap matrix OC, satisfying the condition of no synchronized chain between them. Collectively, Fig. 1(d) depicts a typical case of RS identified by the NCOPA approach.

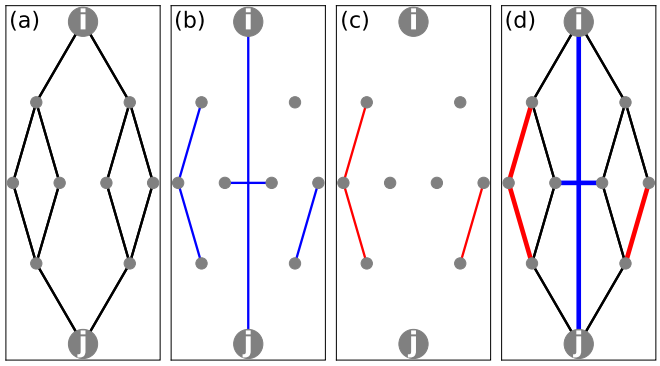

FIG. 1. The noncomplete overlapping path algorithm for detecting RS where the black, blue, and red lines represent the SC, FC, and OC connections, respectively. Panels (a)–(c) represent the networks of SC, FC, and OC, respectively, and panel (d) integrates all the connections of panels (a)–(c) together.

A characteristic feature of the NCOPA approach is that it is based on link connectivity, regardless of whether it is represented by an adjacency matrix or a weighted matrix. In this sense, the measured RS is the same when using either the simplified adjacency matrix or the naturally weighted matrix, as both share the same connectivity.

III. DETECTING REMOTE SYNCHRONIZATION FROM EMPIRICAL DATA OF BRAIN NETWORKS

As discussed above, human brain dynamically reconfigures its functional organization to support diverse cognitive task performances [37,38]. RSNs exhibit a highly structured architecture that mirrors task-induced activity patterns, thereby enabling accurate predictions of task performance [39,40]. Given that RSN data are relatively easy to acquire experimentally, they represent a robust proxy for investigating brain function. Accordingly, we utilized the RSN dataset from Ref. [41], which examines how the resting brain configures its functional organization to balance segregation and integration demands, thereby optimizing cognitive support. This dataset comprises 833 healthy young adults from the Washington University-University of Minnesota (WU-Minn) Consortium Human Connectome Project [42]. Cortical parcellation was performed using the multimodal parcellation atlas, segmenting the brain into $N = 360$ distinct regions [43]; consequently, the resulting functional brain network consists of 360 nodes. The demographic characteristics of the participants can be represented as follows: The data contain 833 subjects (female = 455, male = 388, age range = 22–36 years), and all of them are healthy young adults.

We begin by analyzing the structural brain networks derived from diffusion tensor imaging data for all participants, i.e., W_{ij}, which denotes the connection weight (or probability)

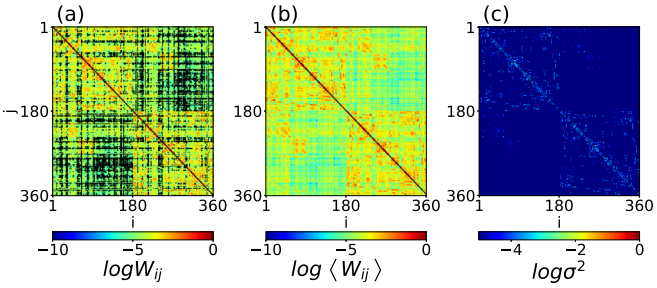

FIG. 2. Weighted connection matrices of brain structural networks from Ref. [41] where all the color bars are taken on the logarithmic scale. (a) Case of the eight-hundredth subject. (b) Case of averaging on all the 833 subjects. (c) The standard deviation of all the 833 subjects.

between region i and region j [43]. Figure 2(a) illustrates the weighted structural connectivity matrix for subject 800 as a representative example, with the color bar presented on a logarithmic scale. The matrix is characterized by high density and heterogeneity. Given individual variability, the specific configuration of W_{ij} differs across subjects. To quantify this variability, we computed the group-level mean $\langle W_{ij}\rangle$ and σ^2 to be the average and standard deviation across all 833 participants. Figures 2(b) and 2(c) depict the spatial distributions of $\langle W_{ij}\rangle$ and σ^2, respectively, both rendered on a logarithmic scale. Notably, Fig. 2(b) reveals a distinct community topology within the averaged structural network. Furthermore, as evidenced by Fig. 2(c), the standard deviation σ^2 is relatively small (on the order of 10^{-3}). We therefore conclude that the overall structural connectivity strength is consistent across subjects, indicating that interindividual variations are quantitatively modest.

We next examined the functional brain networks, quantified by the Pearson correlation coefficients between BOLD time series, denoted as F_{ij} in Eq. (1). These data correspond to cognitive behavioral measures spanning general and domain-specific phenotypes, acquired during nine distinct task paradigms [41]. Figure 3(a) presents the weighted functional connectivity matrix for subject 800. Similar to the structural matrix in Fig. 2(a), this matrix exhibits high density and heterogeneity. To characterize interindividual variability, Figs. 3(b) and 3(c) display the group-averaged functional matrix $\langle F_{ij}\rangle$ and its corresponding standard deviation σ^2,

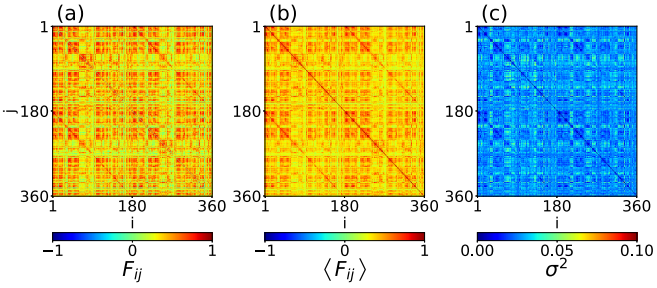

FIG. 3. Weighted connection matrices of brain functional networks from Ref. [41]. (a) Case of the eight-hundredth subject. (b) Case of averaging on all the 833 subjects. (c) The standard deviation of all the 833 subjects.

respectively. Unlike the modular (community) structure observed in the structural average [Fig. 2(b)], the functional average [Fig. 3(b)] appears relatively homogeneous, underscoring the fundamental divergence between structural connectivity and functional connectivity [1]. Furthermore, Fig. 3(c) indicates that the standard deviation σ^2 remains relatively low, suggesting that the overall functional topology is largely conserved across subjects.

Both Figs. 2(a) and 3(a) illustrate that the structural and functional networks are fully connected at the macroscopic level, contrasting with the sparsity observed in microscopic neuronal networks. This discrepancy arises because each ROI encompasses a vast number of neurons; while these neurons predominantly link to a finite subset of ROIs, weak connections to distant regions persist. It is well known that brain neural networks exhibit a small-world topology, where the majority of local connections conserve energy and the minority of long-range connections enable high efficiency, reflecting the principles of segregation and integration [37,38]. This sparse architecture must be preserved at the mesoscopic level of ROIs, as it can be considered a renormalization of the microscopic network. To preserve the biological realism of sparse connectivity, we applied binarization thresholds (S_c for structural, F_c for functional networks) to remove edges with negligible weights. Specifically, for structural networks, connections were retained only if $W_{ij} > S_c$; likewise, functional connections were preserved if $W_{ij} > F_c$. Consequently, the resulting networks are sparse, leading to nonuniform nodal degrees. The degree distribution $P(k)$ was subsequently calculated for each network, with k being the node's degree.

Building upon the data presented in Figs. 2 and 3, we employed steps (1) and (2) of the NCOPA framework to determine the optimal threshold matrices for structural connectivity and functional connectivity. Here, a key condition is that the degree distribution of structural network should be approximately exponential while that of functional network should be approximately scale-free [1]. By systematically varying the thresholds S_c and F_c, we observed substantial alterations in both the topological structure of the networks and their corresponding degree distributions, $P(k)$. Figure 4(a) illustrates the degree distributions for five representative structural threshold values: $S_c = 0.0001, 0.001, 0.002, 0.004$, and 0.01. In the semilogarithmic insets, the distributions corresponding to intermediate thresholds ($S_c = 0.001, 0.002, 0.004$) conform closely to a Gaussian distribution. This alignment satisfies the theoretical feature identified in Ref. [1], indicating that $S_c = 0.004$ resides within the optimal range. Consequently, we selected $S_c = 0.004$ for subsequent analyses. Similarly, Fig. 4(b) displays the degree distributions for functional thresholds $F_c = 0.1, 0.6, 0.7, 0.8$, and 0.9. The log-log insets reveal that the distributions for $F_c = 0.6, 0.7$, and 0.8 follow an approximate power-law distribution, consistent with the criterion established in Ref. [1]. Therefore, we adopted $F_c = 0.8$ as the optimal functional threshold for the remainder of this study.

Having established the optimal structural and functional threshold matrices, we next applied the complete NCOPA framework to identify RS between node pairs in the empirical dataset from Ref. [41]. Specifically, we fixed the thresholds at their optimal values ($S_c = 0.004$, $F_c = 0.8$) and

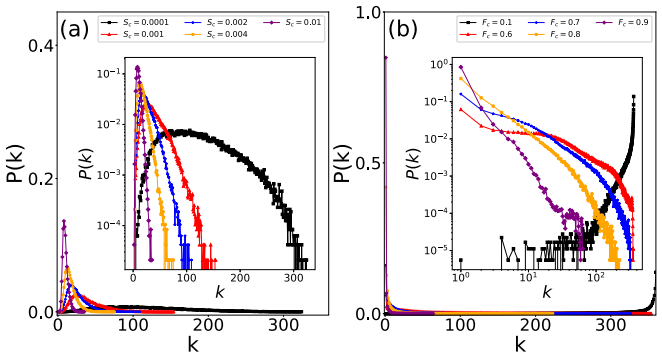

FIG. 4. Degree distributions of the threshold matrices from the data of Figs. 2 and 3. Panel (a) represents the case of the structure threshold matrices SC, where the lines with "black squares," "red triangles," "blue stars," "yellow asterisks," and "pink diamonds" represent the cases of $S_c = 0.0001, 0.001, 0.002, 0.004$, and 0.01, respectively, and the inset shows their corresponding log-linear plots. Panel (b) represents the case of the functional threshold matrices FC, where the lines with "black squares," "red triangles," "blue stars," "yellow asterisks," and "pink diamonds" represent the cases of $F_c = 0.1, 0.6, 0.7, 0.8$, and 0.9, respectively, and the inset shows their corresponding log-log plots.

systematically iterated through all N nodes. For each seed node i, we evaluated all possible target nodes j ($j \neq i$) to determine whether the pair (i, j) satisfied the criteria for RS. Our analysis confirmed the existence of RS in specific node pairs. Figure 5 illustrates two representative examples of RS detected in subject 800, where the network is plotted as a topological network with the seed node i being the center. In Fig. 5(a), node $i = 330$ exhibits three RS partners, whereas node $i = 288$ in Fig. 5(b) has only one RS partner. Furthermore, the topological distances differ: The partners in Fig. 5(a) are separated by two or three steps, while those in Fig. 5(b) are separated by three steps.

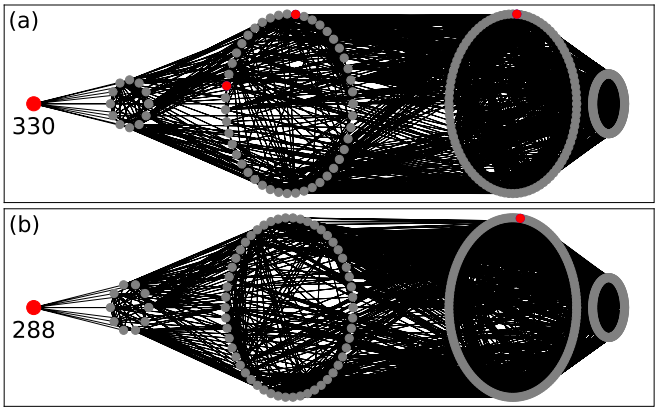

FIG. 5. Representative examples of RS identified in the empirical data of the eight-hundredth subject with $S_c = 0.004$ and $F_c = 0.8$. (a) RS configuration for seed node 330. The topological distance (shortest-path length) between node 330 and its three RS partners is two steps for the first two partners and three steps for the third. (b) RS configuration for seed node 288, exhibiting a single RS partner located three steps away.

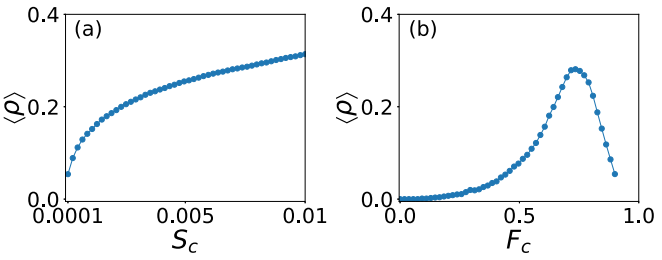

FIG. 6. Dependence of the fraction $\langle\rho\rangle$ of RS nodes on the thresholds S_c and F_c. (a) $\langle\rho\rangle$ vs S_c with $F_c = 0.8$. (b) $\langle\rho\rangle$ vs F_c with $S_c = 0.004$.

Given that the detection of RS is contingent upon the selected thresholds (S_c and F_c), we systematically evaluated their impact on RS prevalence. Let n_{RS} denote the number of unique nodes exhibiting RS with at least one other node in the structural network. Using Fig. 5 as an illustrative example ($S_c = 0.004$ and $F_c = 0.8$), node 330 contributes four instances to n_{RS}, while node 288 contributes two; these were aggregated across the network while eliminating redundant counts. Subsequently, we defined ρ_i as the fraction of RS nodes relative to the total number of regions or nodes N for the subject i:

$$\rho_i = \frac{n_{\mathrm{RS}}}{N}. \tag{2}$$

Then, we implemented this procedure for all 833 subjects to compute the group average

$$\langle\rho\rangle = \frac{1}{N}\sum_{i=1}^{N}\rho_i. \tag{3}$$

Figures 6(a) and 6(b) depict the dependence of $\langle\rho\rangle$ on the thresholds S_c and F_c, respectively, with $F_c = 0.8$ in panel (a) and $S_c = 0.004$ in panel (b). Figure 6(a) reveals that $\langle\rho\rangle$ increases monotonically with S_c. This trend can be attributed to two factors: (1) At low S_c, the structural network retains abundant connections (including long-range connections), facilitating direct connectivity between nodes i and j [Fig. 1(d)]. This reduces the necessity for multistep relay pathways, thereby decreasing the incidence of RS. (2) Conversely, higher S_c values yield sparser networks by pruning weaker connections. This sparsity limits the overlap between structural and functional connectivity pathways, thereby increasing the likelihood of RS configurations.

More notably, Fig. 6(b) exhibits a peak at $F_c \approx 0.75$, which aligns closely with our previously selected optimal threshold of $F_c = 0.8$ [Fig. 4(b)], thereby validating our threshold selection strategy. The nonmonotonic relationship between $\langle\rho\rangle$ and F_c can be explained as follows: (1) At low F_c values, the functional network is densely connected. This high density increases the probability of overlap between structural and functional connections, leaving fewer instances where functional links exist without structural support—precisely the condition required for RS. Thus, $\langle\rho\rangle$ remains low. (2) Conversely, at excessively high F_c values, the functional network becomes too sparse. Even long-range functional connections are pruned, drastically reducing the chance that any two nodes i and j are functionally linked. Consequently, the scarcity of

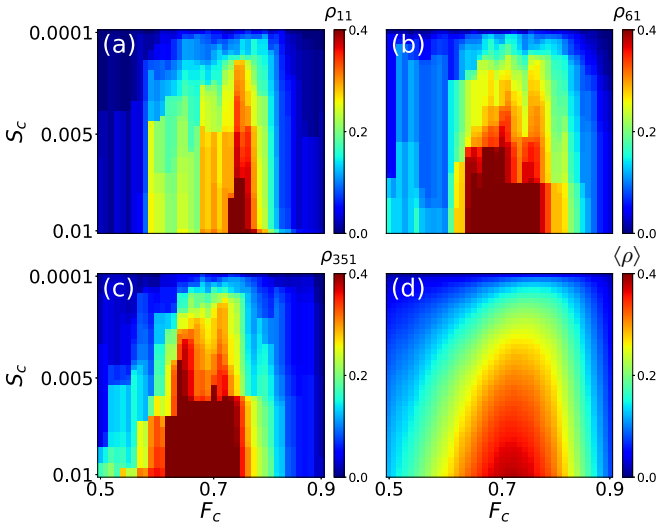

FIG. 7. Phase diagrams of ρ_i and its average $\langle\rho\rangle$ in the phase plane of F_c and S_c. Panels (a)–(c) represent three typical cases of all 833 subjects, i.e., ρ_{11}, ρ_{61}, and ρ_{351}. Panel (d) represents the case of the averaged $\langle\rho\rangle$.

functional connections also leads to a lower fraction of RS. In summary, an intermediate F_c balances structural sparsity with functional integration, maximizing the occurrence of RS and giving rise to the peak observed in Fig. 6(b).

Figures 6(a) and 6(b) illustrate specific cases with fixed parameters $F_c = 0.8$ and $S_c = 0.004$, respectively. To comprehensively characterize RS, we examine parameter spaces beyond these fixed values and calculate ρ_i for all 833 subjects. We find that the phase diagrams of ρ_i are largely consistent across cases, suggesting that the detected RS patterns are stable. As examples, Figs. 7(a)–7(c) illustrate the phase diagrams of ρ_i for three representative cases, i.e., ρ_{11}, ρ_{61}, and ρ_{351}, as a function of F_c and S_c. In contrast, Fig. 7(d) presents the phase diagram of $\langle\rho\rangle$, which exhibits a markedly smoother profile compared to those in panels (a)–(c). These diagrams reveal an optimal region where the fraction of RS nodes is maximized, indicating that the appropriate selection of thresholds is critical for detecting RS in brain activities.

To elucidate the biological significance of the detected RS pairs, it is essential to identify nodes that are recurrently involved in RS. To this end, we performed a statistical analysis on RS nodes at $S_c = 0.004$ and $F_c = 0.8$. For each subject, we quantified the involvement of individual nodes by counting their occurrences across distinct RS node pairs. Crucially, this tally reflects the number of unique RS pairs a node participates in, rather than the binary indicator n_{RS} (where a node is counted once regardless of its frequency). Thus, a node with degree k participating in m pairs contributes m counts to the distribution. We computed these data for all 833 subjects and then obtain their degree distribution $P_{\mathrm{RS}}(k)$, plotted as red points in Fig. 8(a). For comparison, the standard degree distribution $P(k)$, averaged across all subjects, is shown as blue points. The close alignment between the red and blue curves indicates that nodes with higher degrees are preferentially engaged in RS formations.

However, an intriguing pattern emerges when examining the topological distance D_{ij} between RS node pairs (i and j).

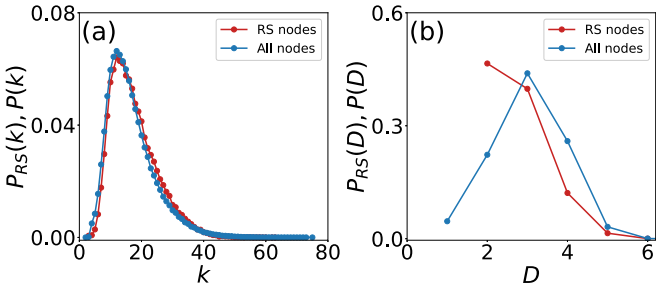

FIG. 8. Distributions of RS nodes on their degrees and topological distances with $S_c = 0.004$ and $F_c = 0.8$. (a) Degree distributions for RS nodes [red, $P_{\mathrm{RS}}(k)$] and all nodes [blue, $P(k)$]. (b) Topological distance distributions for RS nodes [red, $P_{\mathrm{RS}}(D)$] and all nodes [blue, $P(D)$].

For the thresholds of $S_c = 0.004$ and $F_c = 0.8$, we computed the pairwise distances D between each individual pair of RS nodes for all 833 subjects to construct a distance distribution $P_{\mathrm{RS}}(D)$, plotted as red points in Fig. 8(b). For comparison, we also calculated the network distance distribution $P(D)$ (blue points), defined as the distribution of shortest-path lengths from each node to all other $N-1$ nodes. Notably, $P_{\mathrm{RS}}(D)$ exhibits a monotonically decreasing profile compared to the unimodal distribution of $P(D)$. This feature suggests that RS pairs are most probably appeared among those nodes with topological distance of two or three steps, a topological feature consistent with the organization of cognitive circuits, which often integrate functionally different cortical regions such as the attention, frontoparietal, default-mode networks, etc. [22–25,49]. This finding also provide an evidence to support the paradigmatic model of star graph for RS [4].

To clarify the algorithmic cost, we recommend reporting the computational complexity and scalability of NCOPA. Our results show that the calculation takes just a few hours on a standard workstation when all the empirical data are properly preprocessed. Thus, this computational demand remains reasonable even for larger or denser connectomes.

IV. EXTENSION TO DYNAMICAL OSCILLATORS

While the NCOPA approach was initially developed for empirical brain network data, it may also be effective for other complex networks. If so, it would become a general-purpose method, thereby substantially advancing our understanding of RS. However, its generalizability to such networks remains to be verified. To address this, we retained the brain structural connectivity matrix but replaced the experimental time series $x(i,t)$ in Eq. (1) with synthetic data generated from a dynamical model. This generates an equivalent functional network driven by network dynamics. Specifically, we modeled each node using the Kuramoto phase oscillator:

$$\dot{\theta}_i = \omega_i + \lambda \sum_{j=1}^{N} W_{ij} \sin(\theta_j - \theta_i), \tag{4}$$

where $i = 1, \ldots, N$, λ is the coupling strength, and ω_i represents the natural frequency of node i, sampled from a Gaussian distribution $N(u, \sigma^2)$. For this study, we fixed the parameters at $u = \langle\omega_i\rangle = 10.0$ and $\sigma^2 = 0.1$. By substituting the phase

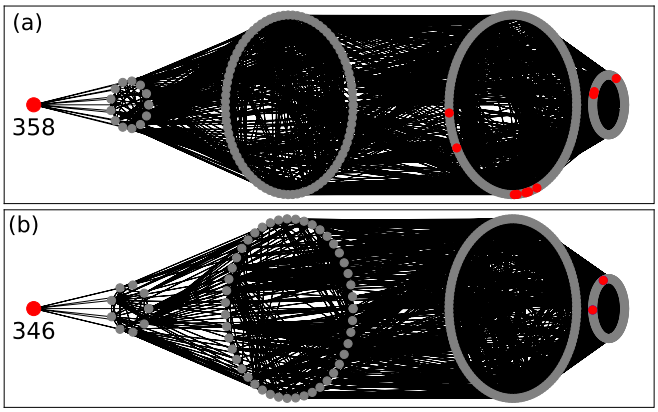

FIG. 9. Two typical RS identified in the brain network of subject 800 using the nodal dynamics defined in Eq. (4). The structural threshold is $S_c = 0.004$ and the functional threshold is $F_c = 0.8$. (a) RS of node 358, where the topological distance to its RS partners is either three or four steps. (b) RS of node 346, where the topological distance to its RS partners is four steps.

time series θ_i from Eq. (4) into Eq. (1), we reconstructed the resulting functional network topology.

The dynamics described by Eq. (4) are highly dependent on the coupling strength λ. At low λ, the oscillators remain uncorrelated; at intermediate λ, the system exhibits partial synchronization; and at high λ, full synchronization occurs. Consequently, if the system possesses the potential to generate RS, this state must manifest within the intermediate coupling regime. To verify this, we utilized the structural network of subject 800 ($S_c = 0.004$) and set the functional threshold at $F_c = 0.8$. Through numerical simulations, we indeed observed the emergence of RS. Figure 9 illustrates two typical RS patterns at $\lambda = 0.28$: panel (a) corresponds to a topological distance of three steps, while panel (b) corresponds to four steps. A comparison with Figs. 5(a) and 5(b) reveals striking similarities, confirming that the NCOPA approach can successfully detect RS in systems of networked oscillators.

V. A BRIEF THEORETICAL ANALYSIS

Building on the nodal dynamics of Eq. (4), we proceed to develop a theoretical explanation for the emergence of RS. For a pair of structurally unconnected nodes i and j, the governing equations are given by

$$\begin{aligned}\dot{\theta}_i &= \omega_i + \lambda \sum_{k=1}^{N} W_{ik} \sin(\theta_k - \theta_i),\\ \dot{\theta}_j &= \omega_j + \lambda \sum_{k=1}^{N} W_{jk} \sin(\theta_k - \theta_j).\end{aligned} \tag{5}$$

The evolution of their phase difference can be expressed as

$$\dot{\theta}_i - \dot{\theta}_j = \omega_i - \omega_j + \lambda \sum_{k=1}^{N} [W_{ik} \sin(\theta_k - \theta_i) - W_{jk} \sin(\theta_k - \theta_j)]. \tag{6}$$

Let $\Delta\theta_{ij} \equiv \theta_i - \theta_j$. When the two nodes i and j are RS, we have $\Delta\theta_{ij} = 0$, which gives

$$\omega_j - \omega_i = \lambda \sum_{k=1}^{N} [W_{ik} \sin(\theta_k - \theta_i) - W_{jk} \sin(\theta_k - \theta_j)]. \tag{7}$$

That is, RS can emerge when the coupling interaction between nodes i and j compensates for their natural frequency mismatch. This yields the following condition for RS:

$$\lambda \geqslant \lambda_1 \equiv \frac{\omega_j - \omega_i}{\sum_{k=1}^{N} [W_{ik} \sin(\theta_k - \theta_i) - W_{jk} \sin(\theta_k - \theta_j)]}. \tag{8}$$

Conversely, for two structurally unconnected nodes i and j to exhibit RS, at least two neighboring nodes along every connecting path must remain unsynchronized. Otherwise, if all nodes on a path synchronize for $\lambda \geqslant \lambda_1$, nodes i and j would become synchronized, precluding the formation of RS. Suppose nodes p and q are the specific unsynchronized pair on the path between i and j. Since p and q follow the dynamics of Eq. (5), we have

$$\dot{\theta}_p - \dot{\theta}_q = \omega_p - \omega_q + \lambda \sum_{k=1}^{N} [W_{pk} \sin(\theta_k - \theta_p) - W_{qk} \sin(\theta_k - \theta_q)]. \tag{9}$$

Let $\Delta\theta_{pq} \equiv \theta_p - \theta_q$. When the two nodes p and q are not synchronized, we have $\Delta\dot{\theta}_{pq} \neq 0$, which gives

$$\lambda \leqslant \lambda_2 \equiv \frac{\omega_q - \omega_p}{\sum_{k=1}^{N} [W_{pk} \sin(\theta_k - \theta_p) - W_{qk} \sin(\theta_k - \theta_q)]}. \tag{10}$$

Consequently, the necessary condition for RS requires the coupling strength λ to satisfy both Eqs. (8) and (10) simultaneously. Since the dynamics of nodes p and q and their adjacency matrices in these equations are intrinsically linked, the emergence of RS is contingent upon the precise matching of multiple factors: local network topology, the thresholds F_c and S_c, and the coupling strength λ. In this regard, the conditions for RS vary for each node pair, leading to RS nodes appearing heterogeneously across the network. This heterogeneity may explain why cognitive networks exhibit dynamic reconfiguration during daily activities.

VI. DISCUSSIONS AND CONCLUSIONS

RS has emerged as a topic of significant interest in the fields of nonlinear science and complex networks. While early theoretical work primarily relied on the star-graph topology [4], subsequent investigations have extended to interconnected stars [29], partially coupled starlike structures [44], multistar configurations [31], community-based networks [34,45], and triggered by external drives [33] or noise [46]. Crucially, these theoretical frameworks are universally predicated on a specific assumption: a substantial disparity between the natural frequencies of the hub and leaf nodes. However, this prerequisite lacks empirical validation in neurophysiological data. In contrast, the NCOPA approach introduced herein circumvents this limitation. It provides a generalizable and robust framework for detecting RS without requiring specific frequency mismatches, making it uniquely suited for analyzing real-world complex systems such as brain

networks. Specifically, unlike graph-based or dynamical approaches that are restricted to star or starlike graphs, NCOPA can measure RS between distant nodes and is readily applicable to empirical data. This advantage carries considerable practical importance, since the emergence and variation of cognitive networks have always served as the starting point for RS research.

So far, we have primarily focused on detecting RS in empirical brain network data. A closely related question is what causes pairs of nodes to become remotely synchronized in networks where both structural and functional edges are threshold dependent. To address this, we first examine firing propagation at the microscopic level of neural networks. At this level, recent studies have identified, alongside normal diffusive firing propagation, an abnormal phenomenon termed remote firing propagation. Here, the firing of a source neuron propagates to a distant neuron without requiring the intermediate neurons to fire [47–49]. The underlying reason is that each target neuron connects to the source neuron via multiple parallel pathways, thereby integrating inputs from all of them. When the summed influence exceeds the firing threshold, the target neuron activates regardless of whether the intermediate neurons are active. Building on this mechanism, we return to the earlier scenario where each node represents an ROI comprising thousands of neurons. At this mesoscopic level, link weights are determined by the collective activity of the majority of neurons within nodes, rather than by every single connection between individual neurons; otherwise, the resulting network would be fully connected. Consequently, RS at the mesoscopic level emerges because the majority of neurons linking two nodes exhibit RS at the microscopic level.

It is important to emphasize that our study focuses on the mesoscopic scale, with nodes representing ROIs rather than individual neurons. This allows us to model nodal dynamics using harmonic oscillators like the Kuramoto model. In contrast, a microscopic approach requires modeling each node as a neuron (e.g., using integrate-and-fire models), for which our current formalism is unsuitable. Moreover, microscopic networks comprise hundreds of billions of units, making the acquisition of time-series data exceptionally challenging.

In conclusion, we investigated RS from the perspective of brain network time series, departing from the star graph and starlike models used in prior studies. We proposed a four-step NCOPA algorithm to measure RS in both empirical time series and dynamical models. The core principle of NCOPA is that recurrent functional connections occur between nodes that are structurally not directly connected, with no intervening chain of synchronized nodes linking them. We demonstrated that the thresholds F_c and S_c are critical determinants of RS, and that optimal values exist to align with empirical observations. Furthermore, we showed that this approach generalizes to arbitrary complex networks. Our findings provide a comprehensive understanding of the brain's functional principles in supporting diverse cognitive demands and advance theoretical frameworks in network neuroscience.

ACKNOWLEDGMENTS

This work was partially supported by STI2030-Major Project No. 2021ZD0202600 and the NNSF of China under Grants No. 12575037 and No. 42461144209.

DATA AVAILABILITY

The data that support the findings of this article are openly available [50].

[1] V. M. Eguiluz, D. R. Chialvo, G. A. Cecchi, M. Baliki, and A. V. Apkarian, Scale-free brain functional networks, Phys. Rev. Lett. **94**, 018102 (2005).

[2] E. Bullmore and O. Sporns, Complex brain networks: Graph theoretical analysis of structural and functional systems, Nat. Rev. Neurosci. **10**, 186 (2009).

[3] F. Varela, J.-P. Lachaux, E. Rodriguez, and J. Martinerie, The brainweb: Phase synchronization and large-scale integration, Nat. Rev. Neurosci. **2**, 229 (2001).

[4] A. Bergner, M. Frasca, G. Sciuto, A. Buscarino, E. J. Ngamga, L. Fortuna, and J. Kurths, Remote synchronization in star networks, Phys. Rev. E **85**, 026208 (2012).

[5] M. J. Panaggio and D. M. Abrams, Chimera states: Coexistence of coherence and incoherence in networks of coupled oscillators, Nonlinearity **28**, R67 (2015).

[6] S. Majhi, B. K. Bera, D. Ghosh, and M. Perc, Chimera states in neuronal networks: A review, Phys. Life Rev. **28**, 100 (2019).

[7] Z. Wang and Z. Liu, A brief review of chimera state in empirical brain networks, Front. Physiol. **11**, 724 (2020).

[8] F. Parastesh, S. Jafari, H. Azarnoush, Z. Shahriari, Z. Wang, S. Boccaletti, M. Perc, Chimeras, Phys. Rep. **898**, 1 (2021).

[9] T. Wu, X. Zhang, and Z. Liu, Understanding the mechanisms of brain functions from the angle of synchronization and complex network, Front. Phys. **17**, 31504 (2022).

[10] Z. Liu, Physical mechanisms of human brain functions, Quant. Biol. **13**, e70 (2025).

[11] S. B. Eickhoff, B. T. Thomas Yeo, and S. Genon, Imaging-based parcellations of the human brain, Nat. Rev. Neurosci. **19**, 672 (2018).

[12] P. Fries, A mechanism for cognitive dynamics: Neuronal communication through neuronal coherence, Trends Cognit. Sci. **9**, 474 (2005).

[13] J. Gross, F. Schmitz, I. Schnitzler, K. Kessler, K. Shapiro, B. Hommel, and A. Schnitzler, Modulation of long-range neural synchrony reflects temporal limitations of visual attention in humans, Proc. Natl. Acad. Sci. USA **101**, 13050 (2004).

[14] F. Crick and C. Koch, Some reflections on visual awareness, Cold Spring Harbor Symp. Quant. Biol. **55**, 953 (1990).

[15] M. Volgushev, S. Chauvette, M. Mukovski, and I. Timofecv, Precise long-range synchronization of activity and silence in neoconical neurons during slow-wave sleep, J. Neurosci. **26**, 5665 (2006).

[16] J. F. Hipp, A. K. Engel, and M. Siegel, Oscillatory synchronization in large-scale cortical networks predicts perception, Neuron **69**, 387 (2011).

[17] L. G. Dominguez, R. A. Wennberg, W. Gaetz, D. Cheyne, O. C. Snead, and J. L. P. Velazquez, Enhanced synchrony in

epileptiform activity? Local versus distant phase synchronization in generalized seizures, J. Neurosci. **25**, 8077 (2005).
[18] P. J. Uhlhaas and W. Singer, Abnormal neural oscillations and synchrony in schizophrenia, Nat. Rev. Neurosci. **11**, 100 (2010).
[19] S. Ansarinasab, F. Ghassemi, Z. Tabanfar, and S. Jafari, Investigation of phase synchronization in functional brain networks of children with ADHD using nonlinear recurrence measure, J. Theor. Biol. **560**, 111381 (2023).
[20] S. Ansarinasab, A. Bayani, F. Parastesh, F. Ghassemi, K. Rajagopal, and S. Jafari, Transition to synchronization in functional brain networks of children suffering from ADHD, Brain Struct. Funct. **230**, 82 (2025).
[21] G. Buzsaki, *Rhythms of the Brain* (Oxford University Press, New York, 2006).
[22] G. Deco, A. Ponce-Alvarez, D. Mantini, G. L. Romani, P. Hagmann, and M. Corbetta, Restingstate functional connectivity emerges from structurally and dynamically shaped slow linear fluctuations, J. Neurosci. **33**, 11239 (2013).
[23] D. D. Garrett, G. R. Samanez-Larkin, S. W. S. MacDonald, U. Lindenberger, A. R. McIntosh, and C. L. Grady, Moment-to-moment brain signal variability: A next frontier in human brain mapping?, Neurosci. Biobehav. Rev. **37**, 610 (2013).
[24] A. Das, C. de Los Angeles, and V. Menon, Electrophysiological foundations of the human default-mode network revealed by intracranial-EEG recordings during resting-state and cognition, NeuroImage **250**, 118927 (2022).
[25] D. D. Garrett, N. Kovacevic, A. R. McIntosh, and C. L. Grady, The modulation of bold variability between cognitive states varies by age and processing speed, Cereb. Cortex **23**, 684 (2013).
[26] T. J. Buschman and E. K. Miller, Top-down versus bottom-up control of attention in the prefrontal and posterior parietal cortices, Science **315**, 1860 (2007).
[27] O. Sporns, D. R. Chialvo, M. Kaiser, and C. C. Hilgetag, Organization, development and function of complex brain networks, Trends Cognit. Sci. **8**, 418 (2004).
[28] J. Lacerda, C. Freitas, and E. Macau, Multistable remote synchronization in a star-like network of non-identical oscillators, Appl. Math. Modell. **69**, 453 (2019).
[29] L. Kang, Z. Wang, S. Huo, C. Tian, and Z. Liu, Remote synchronization in human cerebral cortex network with identical oscillators, Nonl. Dyn. **99**, 1577 (2020).
[30] Z. Yang, D. Chen, Q. Xiao, and Z. Liu, Phase frustration induced remote synchronization, Chaos **32**, 103125 (2022).
[31] R. Gao, Z. Lu, and Z. Liu, Bridge links induced remote synchronization in multiple connected star graphs, Chaos, Solitons Fractals **186**, 115223 (2024).
[32] R. Gao and Z. Liu, Distant remote synchronization in multiple connected star graphs, Phys. Rev. E **112**, 044206 (2025).
[33] S. Huo, Z. Huang, N. Yao, and Z. Liu, Remote synchronization induced by external signals in star networks, Chaos, Solitons Fractals **196**, 116345 (2025).
[34] Z. Lu, D. Chen, R. Gao, S. Boccaletti, L. Minati, and Z. Liu, A remote synchronization model of community networks with homogeneous frequencies, Chaos, Solitons Fractals **194**, 116134 (2025).
[35] L. V. Gambuzza, A. Cardillo, A. Fiasconaro, L. Fortuna, J. Gomez-Gardenes, and M. Frasca, Analysis of remote synchronization in complex networks, Chaos **23**, 043103 (2013).
[36] C. J. Honey, O. Sporns, L. Cammoun, X. Gigandet, J. P. Thiran, R. Meuli, and P. Hagmann, Predicting human resting-state functional connectivity from structural connectivity, Proc. Natl. Acad. Sci. USA **106**, 2035 (2009).
[37] O. Sporns, *Networks of the Brain* (MIT Press, Cambridge, 2010).
[38] D. S. Bassett and E. T. Bullmore, Small-world brain networks revisited, Neuroscientist **23**, 499 (2017).
[39] K. Hilger, M. Fukushima, O. Sporns, and C. J. Fiebach, Temporal stability of functional brain modules associated with human intelligence, Hum. Brain Mapp. **41**, 362 (2020).
[40] A. H. C. Fong *et al.*, Dynamic functional connectivity during task performance and rest predicts individual differences in attention across studies, NeuroImage **188**, 14 (2019).
[41] R. Wang, M. Liu, X. Cheng, Y. Wu, A. Hildebrandt, and C. Zhou, Segregation, integration, and balance of large-scale resting brain networks configure different cognitive abilities, Proc. Natl. Acad. Sci. USA **118**, e2022288118 (2021).
[42] D. C. Van Essen *et al.*, The WU-Minn Human Connectome Project: An overview, NeuroImage **80**, 62 (2013).
[43] M. F. Glasser *et al.*, A multi-modal parcellation of human cerebral cortex, Nature (London) **536**, 171 (2016).
[44] Z. Yang, D. Chen, G. Hu, and Z. Liu, Partial remote synchronization in star-like networks with partial connections among leaf nodes, Phys. Rev. Res. **5**, 043253 (2023).
[45] H. Cao, Z. Yang, and Z. Liu, Remote synchronization in multi-layered community networks with star-like topology, Chaos, Solitons Fractals **166**, 112893 (2023).
[46] S. Huo, N. Yao, Z. Huang, C. Grebogi, and Z. Liu, Noise-induced remote synchronization in star networks, Chaos, Solitons Fractals **207**, 118045 (2026).
[47] Z. Wang and Z. Liu, Effect of remote signal propagation in an empirical brain network, Chaos **31**, 063126 (2021).
[48] Q. Shen and Z. Liu, Remote firing propagation in the neural network of *C. elegans*, Phys. Rev. E **103**, 052414 (2021).
[49] D. Chen, R. Gao, Z. Yang, S. Huo, and Z. Liu, Firing propagation in empirical cognitive networks of human brain, Phys. Rev. Res. **7**, 013116 (2025).
[50] https://www.humanconnectome.org/study/hcp-young-adult.